Chapter 7
Peptide-Based Supramolecular Chemistry

Qianli Zou, Kai Liu, Manzar Abbas and Xuehai Yan

Abstract Supramolecular chemistry of highly important biomolecules and bioinspired molecules has attracted tremendous interest due to its acknowledged importance in construction of novel functional materials and in revealing the mechanisms of formation and evolution of natural living organisms. As one kind of representative biomolecules, peptides are among the most appealing programmable building blocks for supramolecular self-assembly. In this chapter, we present recent progresses in supramolecular chemistry of self-assembling aromatic dipeptides, including self-assembly of aromatic dipeptides and co-assembly of aromatic dipeptides with various functional molecular motifs, such as porphyrins, azobenzenes, photosensitizers, polyoxometalates, quantum dots, and glutaraldehyde. Particularly, hierarchical self-assembly of peptides and structural transition of the self-assembled peptide architectures are in-depth discussed in controllable fabrication of peptide materials along with revealing the non-covalent interactions that determine the self-assembly and the structure–property relationships of the formed peptide materials. Also, the applications of peptide-based supramolecular materials as optical waveguiding materials, biomimetic energy materials, and biomaterials are highlighted, providing an increased understanding of the role of peptide-based supramolecular chemistry in construction of novel functional materials.

Keywords Peptide · Supramolecular chemistry · Hierarchical self-assembly · Aromatic dipeptide · Optical waveguiding peptide crystal · Biomimetic photocatalysis

Q. Zou · K. Liu · M. Abbas · X. Yan (✉)
State Key Laboratory of Biochemical Engineering, Institute of Process Engineering, Chinese Academy of Sciences, 100190 Beijing, China
e-mail: yanxh@ipe.ac.cn
URL: http://www.yan-assembly.org/

Q. Zou · X. Yan
Center for Mesoscience, Institute of Process Engineering, Chinese Academy of Sciences, 100190 Beijing, China

K. Liu · M. Abbas
University of Chinese Academy of Sciences, 100049 Beijing, China

J. Li (ed.), *Supramolecular Chemistry of Biomimetic Systems*,
DOI 10.1007/978-981-10-6059-5_7

7.1 Introduction

Supramolecular self-assembly is a ubiquitous phenomenon in naturally evolving living systems [1–3]. Numerous functional structures and materials in living organisms are formed by self-assembly of biomolecules such as peptides, proteins, lipids, DNAs, and saccharides [4–6], through non-covalent intramolecular and intermolecular interactions [7]. Common non-covalent interactions including hydrogen bonding, π–π stacking, hydrophobic effect, electrostatic interactions, and van der Waals forces [8]. Inspired by naturally occurring self-assembly, supramolecular self-assembly of biomolecules based on non-covalent interactions and biomimetic principles is emerging as an efficient and elegant method to construct functional materials [9–12]. Such materials not only show ordered structures ranging from molecular scale to nanoscale, even to microscale, but also possess fantastic physical, chemical, and biological properties, enabling them as competitive candidates for various applications such as biomaterials, electronic materials, renewable energy, and biomedicine [13–17]. In the bottom-up process of self-assembly, the organization of building blocks can be readily tuned by manipulation of the non-covalent interactions through physical or chemical means [18]. Also, co-assembly of distinctly different building blocks provides an easy but highly efficient way to create nanomaterials with more sophisticated structures and properties [19–23]. Moreover, the self-assembled materials can be endowed with a variety of morphological transitions by incorporation of responsive groups into the building blocks, resulting in control of the structures and properties of the materials on demand in applications [24, 25].

Among natural and nature-derived biomolecules, peptides are appealing building blocks for supramolecular chemistry due to their simple structures, flexibility in sequence manipulation, relatively high stability along with good biodegradability, high biocompatibility, and ease of production on a large scale [26, 27]. The 20 natural amino acids offer enormous sequence space for exploring proper building blocks toward specific self-assembling properties based on their diversity in charge, hydrophobicity, and polarity [28]. Unnatural amino acids have also been incorporated into the peptide sequences to increase the diversity of self-assembling peptides and the complexity of self-assembled materials [29]. Other than the primary structures defined by the sequence of amino acids, peptides as self-assembling building blocks are also characterized by their secondary structures. Secondary structures of peptides can serve as building blocks for higher levels of self-assembly [30, 31]. Hence, peptides are particularly suitable for hierarchical assembly, the most powerful yet challenging tool to nanoengineer functional materials. In the formation of secondary and higher levels of peptide structures, hydrogen bonding, mainly from polar amide, amino, and carboxyl groups in the backbone and side chains of peptides, is recognized as an important and in many situations dominating driving force due to its universality, selectivity, and directionality.

With the advances of synthetic methods for peptides, especially solid-phase peptide synthesis, a lot of peptides have been designed, synthesized, and applied toward supramolecular self-assembly [32, 33]. Successful peptide self-assembly has been demonstrated by using cyclic peptides, dendritic peptides, polypeptides, amphiphilic peptides, and aromatic dipeptides. In many cases, the sequence of peptides is designed by bioinspired approaches and the structures and properties of the self-assembled materials are highly reminiscent of natural biological systems. Due to their biological inspiration, peptide-based supramolecular materials have shown advantages in various biomedical applications, such as drug delivery, tissue engineering, bone regeneration, antibacterium, imaging, and immunotherapy [34–37]. Since self-assembled peptide-based materials are highly ordered at nanoscale, their properties and functions are not only related with the sequence of amino acids but also are related with their supramolecular nanostructures. Thus, the controllable construction and manipulation of peptide nanostructures are the primary goal in the field of peptide-based supramolecular chemistry. By varying self-assembling peptides and the corresponding non-covalent interactions, supramolecular nanostructures, including nanospheres, nanotubes, nanobelts, nanofibers, and nanogels have been obtained in peptide self-assembly [38, 39]. The non-covalent interactions, thermodynamics, and kinetics in formation of the nanostructures and structure–property relationships of the formed nanomaterials are also acquired [40–42]. In return, these results provide information for revealing the non-covalent interactions of natural peptide and protein based systems.

Aromatic dipeptides, mainly derived from L-Phe-L-Phe (FF), are the simplest peptides that exhibit self-assembling characteristics. Self-assembly of FF is inspired by the formation of amyloid plaques by FF-containing polypeptides in the progress of Alzheimer's disease [43]. In recent years, aromatic dipeptides have been demonstrated as versatile building blocks for supramolecular construction of ordered nanostructures [44, 45]. As compared to other self-assembling peptides, aromatic dipeptides have advantages of simpler molecular structures, lower costs of synthesis, and ease of modification and modulation, which are highly valuable for both reveal of inherent self-assembling mechanisms and manipulation of properties toward specific applications.

In this chapter, we focus on supramolecular chemistry of aromatic dipeptides and their analogs. We first present controlled self-assembly of aromatic dipeptides and the modulation of the self-assembled nanostructures with emphasis on self-assembled peptide crystals with optical waveguiding properties. Then, we discuss co-assembly of aromatic dipeptides with other functional molecules and materials, including porphyrins, azobenzenes, photosensitizers, polyoxometalates (POMs), quantum dots (QDs), and glutaraldehyde (GA). Finally, we highlight the applications of peptide-based nanomaterials in the areas of biomimetic photosystem, photocatalysis, and biomedicine.

7.2 Self-assembly of Peptides

Many ordered nanostructures and macrostructures, such as nanotubes, nanowires, nanobelts, macroporous honeycomb scaffolds, crystals, and mesocrystals can be formed through controlled self-assembly of FF and its analogs. Intriguingly, the self-assembled structures show reversible transitions under stimuli, such as dilution and addition of trace solvent. In addition, peptide crystalline structures show attractive optical waveguiding properties.

7.2.1 Controlled Self-assembly of Peptides

Self-assembly of FF has attracted a lot of attention in nanotechnology since the formation of nanotubes from FF was observed [43]. Further studies discover that other low dimensional nanostructures, such as nanofibrils and nonowires, can be readily obtained by self-assembly of FF in different conditions [46, 47]. To achieve three-dimensional (3D) self-assembled structures of FF, a simple approach toward hierarchical self-assembly of FF was proposed [48]. In this approach, hierarchical spheres with a diameter of 20 μm were obtained simply by adding tetrahydrofuran (THF) to the solution of FF in 1,1,1,3,3,3-hexafluoro-2-propanol (HFIP). Scanning electron microscopy (SEM) reveals that the peony flower-like spheres consist of hundreds of flakes, which are characterized as mesocrystals. The formation of flakes or flower-like spheres can be induced by other solvents, such as 1,4-Dioxane and pyridine. Detailed analyses show that the structures self-assembled from FF by the solvent exchange method are related with the polarity of solvents: nanotubes are formed in hydrogen bond accepter solvents such as water; flakes are formed in hydrogen bond donor solvents; nanofibrils and gels are formed in solvents that provide no sites for hydrogen bonding, such as toluene. Such solvent-related morphology changes are consistent with the fact that the self-assembly of FF is mainly directed by hydrogen bonding and π–π stacking. It is found that the amount of HFIP, which is usually only regarded as a good solvent for dissolving FF, also has a significant impact on the morphology of the self-assembled materials, probably due to its effect on supersaturation of FF in mixed solvent. In addition, temperature also influences the growth of mesocrystals.

Due to the high roughness and surface area, the flower-like spheres exhibit exciting surface-related properties. For example, when a silica substrate covered by the flower-like spheres was further modified by the vapor of fluoroalkylsilane, the modified surface showed excellent superhydrophobicity as well as oleophobicity, suggesting that the hierarchical self-assembled structures of FF can support the formation of antiwetting surfaces. Peptide-based supramolecular materials can serve as templates for construction of functional metallic nanostructures because peptides can be easily removed by solvents or enzymes. A crust of flower-like spheres was obtained by sputtering Au on the surface of flower-like spheres, followed by

removing FF with ethanol [49]. SEM and transmission electron microscopy (TEM) images confirm that the obtained metallic structures consisted of only Au nanoparticles preserve the flower-like morphology. Such hierarchical metallic structures show a remarkable surface enhancement factor for surface-enhanced Raman scattering (SERS) measurements.

Integration of supramolecular self-assembly of FF with the protocol of breath figure is a facile method to generate ordered macrostructures of FF [50]. The formed architectures are honeycomb scaffolds with uniformly distributed and hexagonally organized macropores. The pore sizes and morphology of the scaffolds are readily manipulated by controlling solvent, substrate, air humidity, FF concentration, and air speed. Circular dichroism (CD) and Fourier transform infrared spectroscopy (FTIR) spectra demonstrate that FF in the scaffolds is ordered in the configuration of parallel β-sheet, which is clearly different from the antiparallel configuration of FF organogel formed in toluene. Under ultraviolet (UV) light irradiation, the scaffolds show red-shifted fluorescence, indicating strong π–π stacking and ordered organization of FF in the scaffolds. Significantly, the scaffolds can support the adhesion and growth of human embryo skin fibroblast (ESF) cells, suggesting that such self-assembled macrostructures of FF are promising biomaterials for biomedical applications, such as tissue engineering.

7.2.2 *Structural Transition of Self-assembled Peptide Nanostructures*

Supramolecular self-assembly of the same peptide can form different nanostructures since self-assembly of peptides is relatively susceptible to changes that influence the non-covalent interactions, providing an opportunity to induce structural transition between self-assembled nanostructures. An extensively investigated example is the reversible transition between cationic dipeptide nanotubes and vesicles (Fig. 7.1a) [51]. Cationic dipeptide H-Phe-Phe-NH_2·HCl (CDP), an analog of FF, self-assembles into nanotubes at high concentration and nanovesicles at low concentration (Fig. 7.1b). Hence, the structural transition is easily manipulated by dilution and concentration. CD spectra reveal that the structural transition occurs along with a change in the second structure of CDP (Fig. 7.1c). CD spectra of assembled CDP nanotubes show characteristic signals of α-helical peptides. Also, the existence of π–π stacking among the aromatic side chains and hydrogen bonding among the main chains is indicated by CD results. No significant signal corresponding to second structure of CDP is observed for the form of nanovesicles, suggesting that the transition from nanotubes to nanovesicles is a disassembly process in which electrostatic repulsion possibly plays a key role other than π–π stacking or hydrogen bonding. Moreover, jointed nanovesicles in the shape of a necklace were observed as intermediate structures in the transition between nanotubes and nanovesicles (Fig. 7.1d). An equation presented to demonstrate the

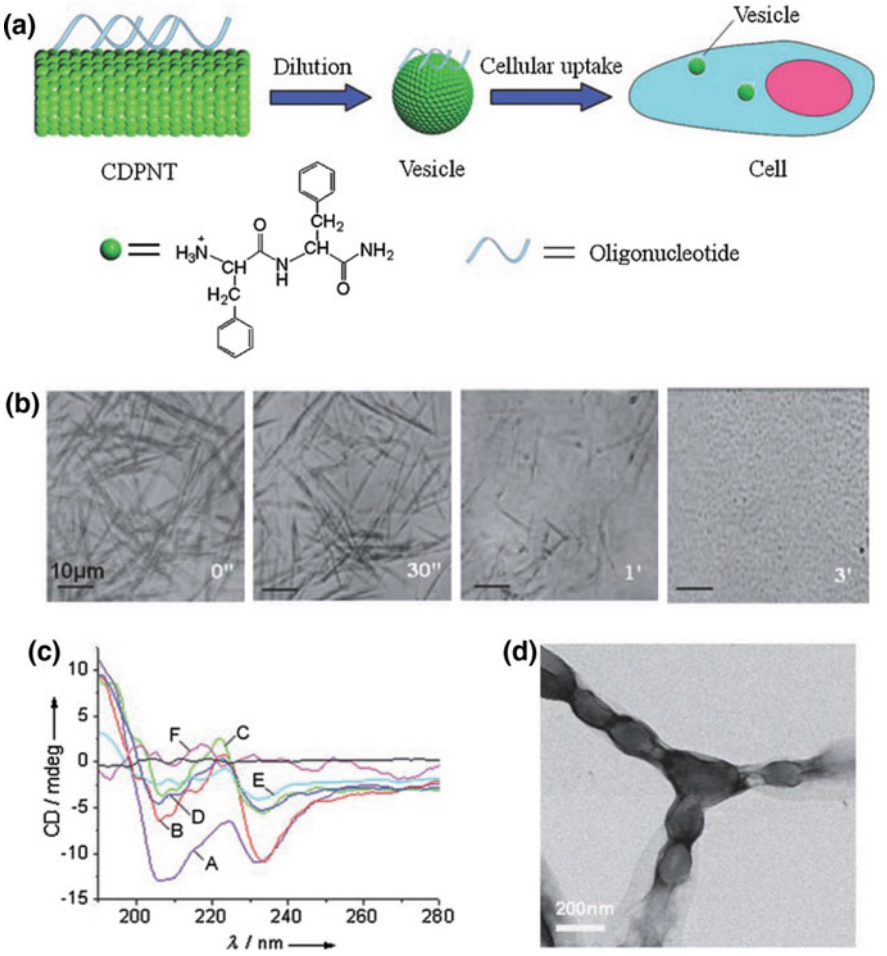

Fig. 7.1 Structural transition of peptide nanostructures. **a** Schematic illustration of structural transition of the CDP nanotubes (CDPNTs) into vehicles for oligonucleotide delivery. **b** Optical images showing the conversion of the CDPNTs into vesicles. **c** CD spectra of the CDPNTs and vesicles at different concentrations (*A* 10, *B* 8, *C* 7, *D* 5, *E* 2, *F* 1 mg mL^{-1}). **d** TEM image of diluted CDPNTs (Reprinted with permission from Ref. [51]. Copyright 2007, Wiley-VCH)

experimental results reveals that the structural transition of peptide-based nanostructures is basically related with the concentration of the building block, the molecular size, and the tension of the solution/aggregate interface [52].

Oligonucleotide delivery has been demonstrated by using CDP nanotubes as carriers for single-stranded DNA (ssDNA) [51]. Negatively charged ssDNA labeled by a fluorescent dye was loaded on the surface of CDP nanotubes through electrostatic interactions. After the nanotubes were changed to nanovesicles under dilution, the fluorescence was found on the obtained nanovesicles, suggesting that

ssDNA was retained with CDP nanostructures in the process of disassembly and reassembly of CDP. When HeLa cells were incubated with ssDNA-bounded nanotubes for 24 h, ssDNA was successfully delivered into the cells. The delivery of ssDNA by CDP nanotubes relies structural transition from nanotubes to nanovesicles upon dilution by cell culture media.

Structural transition from nanofibers to nanobelts was observed in an organogel-based system [53]. The system was constructed by in situ encapsulated of a lanthanide ion (Tb^{3+}) and a photosensitizer (salicylic acid) into FF organogels. SEM imaging reveals that the hybrid organogels consist of small fibers. Due to the presence of Tb^{3+} and salicylic acid, the stability and mechanical strength of the hybrid organogels are lower than that of pure FF organogels formed in toluene. However, the stability and mechanical properties of the hybrid organogels were significantly enhanced by the treatments of heat or water. After the treatments, uniform nanobelts were observed as the main components of the gels, suggesting the structural transition from fibers to nanobelts induced by heat and water. FTIR and X-ray diffraction (XRD) analyses show that the encapsulation of Tb^{3+} and salicylic acid and water treatment have no impact on the secondary structure of FF while the heat treatment induces a change from a β-sheet to a β-turn structure in the organogels. Fluorescence spectra demonstrate that the fluorescence emission of Tb^{3+} is enhanced by synergistic energy transfer from FF and salicylic acid.

7.2.3 Solvent-Induced Structural Transition of Peptide Nanostructures

Self-assembly of peptides in solutions not only involves peptide–peptide interactions but also involves peptide–solvent interactions. Hence, solvent can be a predominant factor to tune peptide nanostructures. The solvent-induced structural transition from organogels to flower-like microcrystals was demonstrated in a system containing FF, toluene, and ethanol [54]. Self-assembly of FF in pure toluene generates organogels. SEM images reveal such organogels consist an entangled network of nanofibers and fiber bundles. In changing pure toluene to a mixture of ethanol and toluene, the self-assembled nanostructures of FF vary from organogels to flower-like microcrystals. SEM images show that the flower-like microcrystals are composed with ribbons. FTIR spectra indicate that the nanostructures obtained in pure toluene and in a low amount of ethanol (10%) show the characteristics of antiparallel β-sheet secondary structures, while the flower-like microcrystals obtained in the presence of a high amount of ethanol have parallel β-sheet secondary structures. The impact of solvent on the morphology is due to different properties of ethanol and toluene: toluene molecules participate in the self-assembly of FF though π–π stacking while ethanol interacts with FF through hydrogen bonding.

Hydrogen bonding is an important interaction involved in self-assembly of biomolecules in biological systems. For example, water-related hydrogen bonding is believed to play a key role in the formation of proteins fibrils in the Alzheimer's disease [55, 56]. Systematic investigation of FF self-assembly in dichloromethane in addition of a trace amount of hydrogen bonding solvent provides a direct evidence for the importance of hydrogen bonding in peptide self-assembly (Fig. 7.2a) [57]. In pure dichloromethane, self-assembly of FF leads to the formation of crystalline structures (Fig. 7.2b). FIIR and XRD results show that crystalline structures are similar with the hexagonal structures in nanotubes and single crystals of FF. When a trace amount of hydrogen bonding solvents such as ethanol, dimethylformamide, or acetone, is added to toluene, long fiber or ribbon structures are formed, suggesting that the assembly of FF in one dimension is induced by directional hydrogen bonding (Fig. 7.2c). In contrast, the addition of n-hexane, a solvent that only shows van der Waals forces with FF, cannot promote fiber structures.

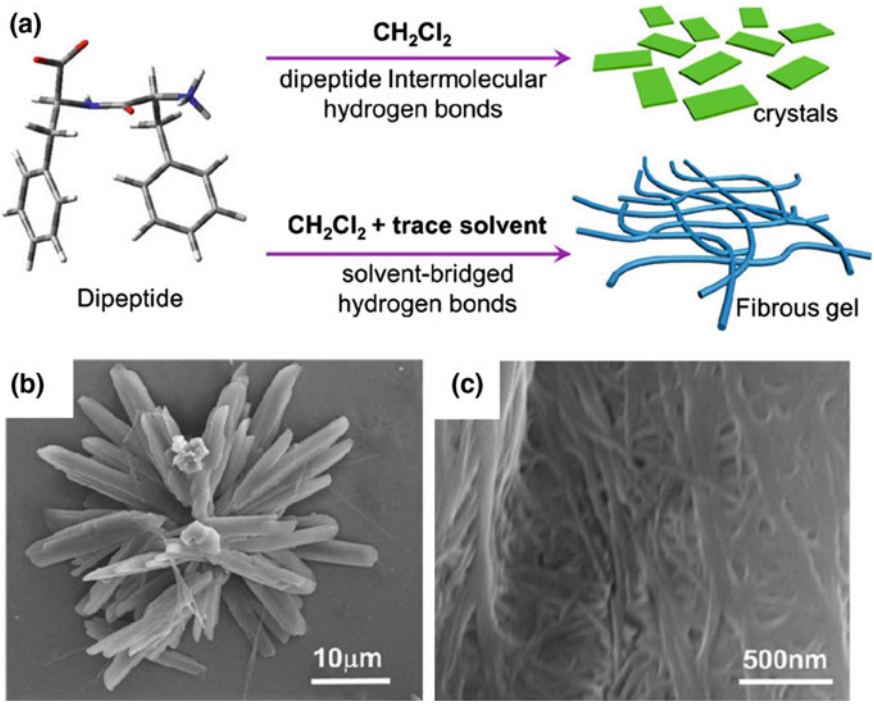

Fig. 7.2 Trace solvent-induced structural transition of FF nanostructures. **a** Schematic illustration of the transition. **b** SEM image of FF/CH_2Cl_2. **c** SEM image of FF/CH_2Cl_2/ethanol (Reprinted with permission from Ref. [57]. Copyright 2016, American Chemical Society)

7.2.4 Self-assembled Peptide Crystals with Optical Waveguiding Properties

The crystalline structures of FF provide platforms for constructing optical waveguiding materials. The waveguide based on self-assembled peptide materials was first demonstrated by aldehyde-induced cyclization and crystallization of FF [58]. To produce the optical waveguiding peptide crystals, organogels were prepared by adding a solution of FF in HFIP into aldehyde-containing toluene. The gels imperceptibly turned into white precipitates in a period of about 1 month. SEM and TEM images demonstrate that the precipitates consist of rectangular platelets, which are composed of anisotropic peptide fiber or ribbon nanostructures. The selected area electron diffraction (SAED) analysis reveals the platelets as single-crystalline peptide platelets. Matrix-assisted laser desorption/ionization time-of-flight (MALDI-TOF) mass spectrometry and ^{1}HNMR spectroscopy show that FF is converted to cyco-Phe-Phe (CPP) in the platelets due to aldehyde-induced cyclization. FTIR and photoluminescence spectra suggest that the formation of platelets is triggered by enhanced hydrogen bonding and π–π stacking interactions. Under excitation at 330–380 nm, the crystalline platelets show blue photoluminescence emission and their ends show remarkably bright spots (Fig. 7.3a, b). When one end of a platelet is excited, bright spots of blue emission can be observed at the other end (Fig. 7.3c, d), suggesting that the light is guided inside the platelet from one end to another. Since the wavelengths of the emission and excitation light are different, the waveguiding based on CPP platelets is a kind of active waveguiding, in which the processes of photoluminescence and waveguiding take place together. Intriguingly, the optical properties of the platelets can be readily tuned by incorporation of other dyes in the process of crystallization. For instance, incorporation of Nile Red into CPP platelets leads to the formation of red light-emitting platelets (Fig. 7.2e, f).

Other than the aldehyde-induced cyclization, CPP platelets can also be prepared by a fast and facile solvothermal approach [59]. It is found that heating the organogels of FF in toluene in sealed vials at a temperature higher than 110 °C generates CPP platelets in 10 min. SEM images reveal that such solvothermally prepared CPP platelets consist of rectangular ultralong nanobelts, similar with those obtained by aldehyde-induced cyclization. Surprisingly, curved crystalline platelets are observed in the precipitates and they show curved optical waveguides upon excitation. Such curved waveguiding along the curved axial of peptide crystalline nanobelts opens a novel way for advanced optical biomaterials.

Self-assembled nanomaterials of FF with crystalline structures also possess optical waveguiding properties. One example is the hexagonal FF microtubes prepared by controlled self-assembly of FF upon solvent thermal annealing [60]. The formation of microtubes from FF is a progress of self-similar-structured growth, which includes the hexagonal packing of FF molecules, ampliative packing

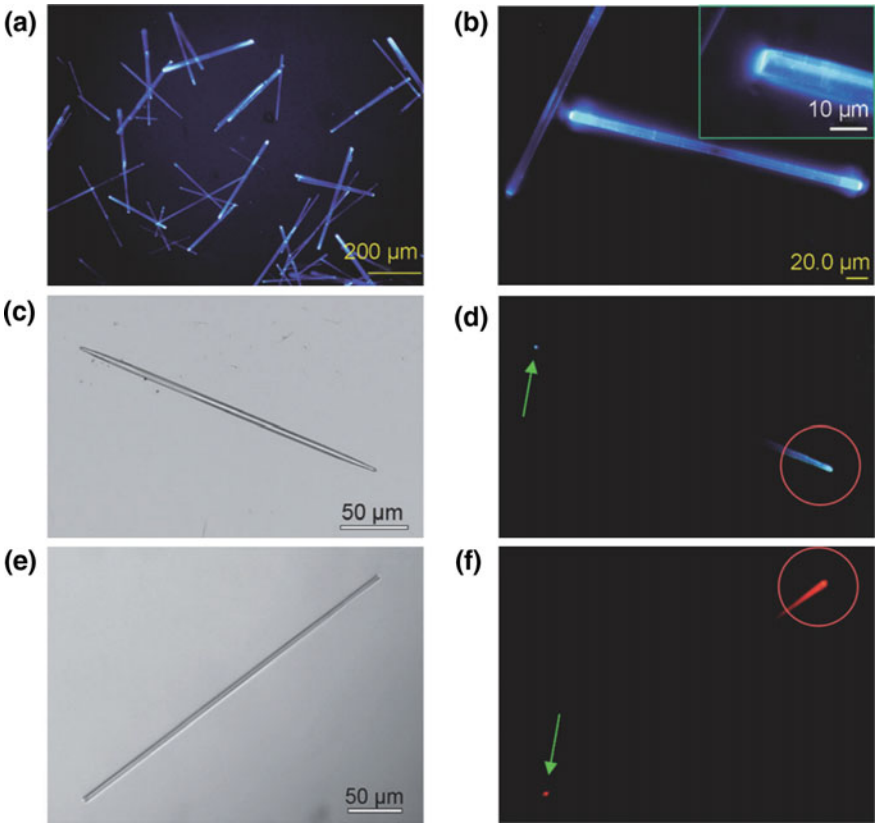

Fig. 7.3 Optical waveguiding of peptide crystals. **a** Photoluminescence image of platelets excited at 330–380 nm. **b** Photoluminescence image of a single platelet. **c** Bright-field image and **d** waveguiding image of a single platelet with local excitation at one end. **e** Bright-field image and **f** waveguiding image of a single platelet incorporating Nile Red dye with local excitation at one end. The *red circle* indicates the excitation area, and the *green arrow* denotes the emission at the other end (Reprinted with permission from Ref. [58]. Copyright 2011, Wiley-VCH)

of the initially formed subunits and the formation of hexagonal nanotubes, and further hierarchical amplification of the nanotubes and the resulting of hexagonal hollow microtubes (Fig. 7.4). Such hierarchically self-assembled FF microtubes show similar XRD patterns with FF single crystals, leading them as promising candidates for active waveguide materials. FF nanofibers, microtubes, and microrods constructed through controlled self-assembly of FF in mixture of HFIP and water with the assistance of ultrasonication also show optical waveguiding characteristics [61]. Moreover, peptide optical waveguide is demonstrated on self-assembled rectangular CDP microtubes and microrods [62].

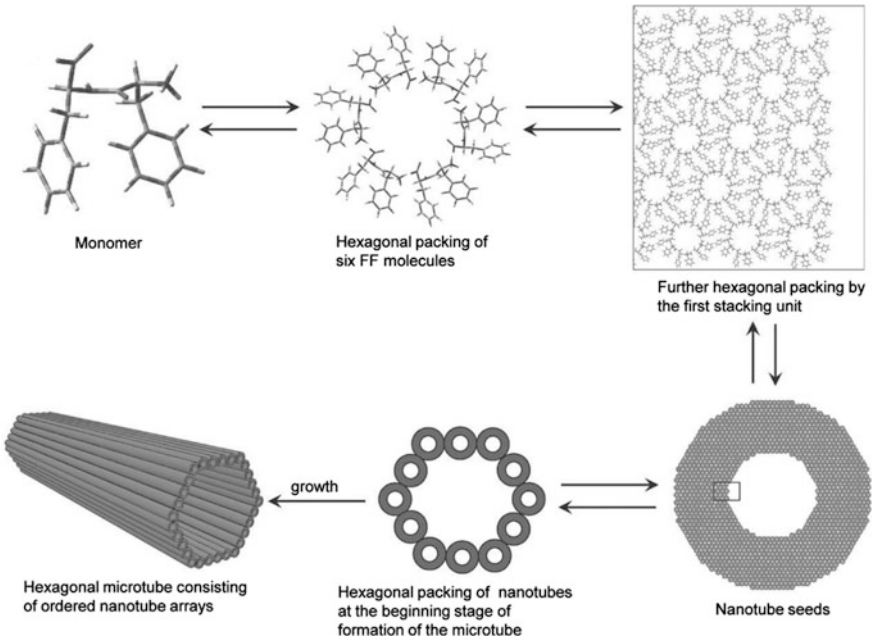

Fig. 7.4 Schematic illustration of the hierarchical self-assembly of FF in the formation of hexagonal FF microtubes through self-similar-structured growth (Reprinted with permission from Ref. [60]. Copyright 2011, Wiley-VCH)

7.3 Peptide-Modulated Self-assembly of Photoactive Molecules

Co-assembly of peptides and other functional molecules provides a simple but efficient strategy for fabrication of functional nanomaterials. Based on such co-assembly strategy, photoactive materials have been constructed through peptide-modulated self-assembly of porphyrins, azobenzenes, and photosensitizers. These photoactive materials show intriguing optical properties due to the ordered arrangement of photoactive molecules inside their nanostructures.

7.3.1 Peptide-Modulated Self-assembly of Porphyrins

Inspired by the natural light-harvesting complexes constructed by chromophores and proteins, a novel and facile strategy has been developed to fabricate light-harvesting architectures via peptide-tuned self-assembly of porphyrins based on the synergy of multiple weak intermolecular interactions [13]. Tetrakis (4-sulfonatophenyl) porphine (TPPS) was chosen as a model light-harvesting

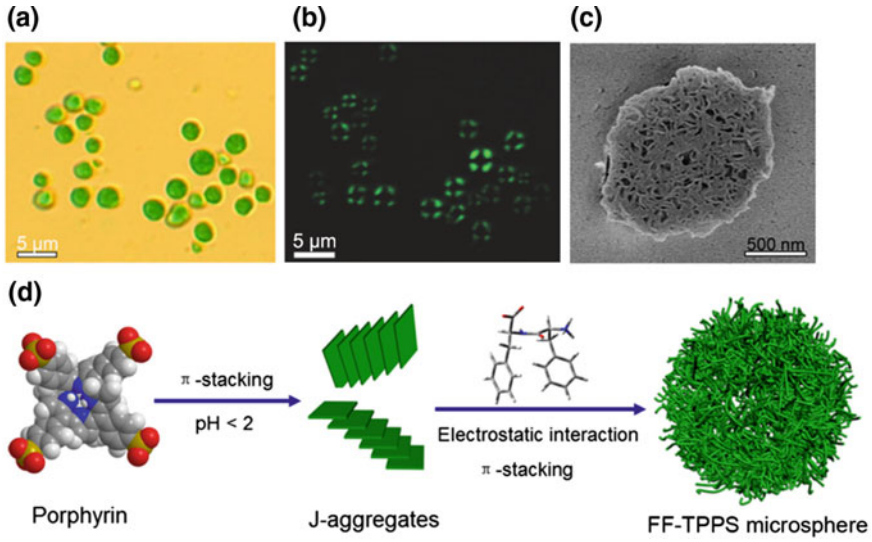

Fig. 7.5 Hierarchical microspheres assembled from FF and TPPS **a** Bright-field image. **b** Polarized image of microspheres when placed between crossed polarizers. **c** SEM image of the cross section of a single microsphere. **d** Proposed hierarchical assembly mechanism (Reprinted with permission from Ref. [63]. Copyright 2014, Wiley-VCH)

porphyrin for its similar photochemical properties to chlorophyll, good water solubility, and capability to self-assemble into higher structures, such as J-aggregation and H-aggregation. Co-assembly of FF and TPPS produces microspheres (Fig. 7.5a) [63]. The microspheres show strong birefringence (Fig. 7.5b), indicating that the TPPS molecules of the microspheres are orderly arranged. SEM images of a single microsphere cross section show that that the microspheres are porous with a multi-compartment interior constructed by many interconnected nanorods (Fig. 7.5c). Uv–vis absorption spectra of the microspheres show a new absorbance peak at 490 nm as compared with that of TPPS, indicating that the TPPS molecules in the microspheres are in J-aggregation. Compared to pure J-aggregated TPPS, this band broadens variously, suggesting that FF perturbs the regular organization of TPPS molecules. The formation of the microspheres is controlled by hierarchical multi-scale self-assembly (Fig. 7.5d). Initially, intermolecular (FF and TPPS) and intramolecular (TPPS) electrostatic interactions combine FF and TPPS molecules together and then co-assemble into nanorods. The nanorods further stack to form microspheres, probably through π–π interactions derived from the benzene ring of FF.

Another light-harvesting model was developed by using hydrophilic L-Lys-L-Lys (KK) to direct the self-assembly of TPPS [64]. In an acid solution, KK and TPPS can co-assemble into long fiber bundles. The fiber bundles are made up of nanorods or nanofibers, which are orderly arranged along the long axis. The fiber bundles show red emission due to the fluorescent of porphyrins. Birefringence

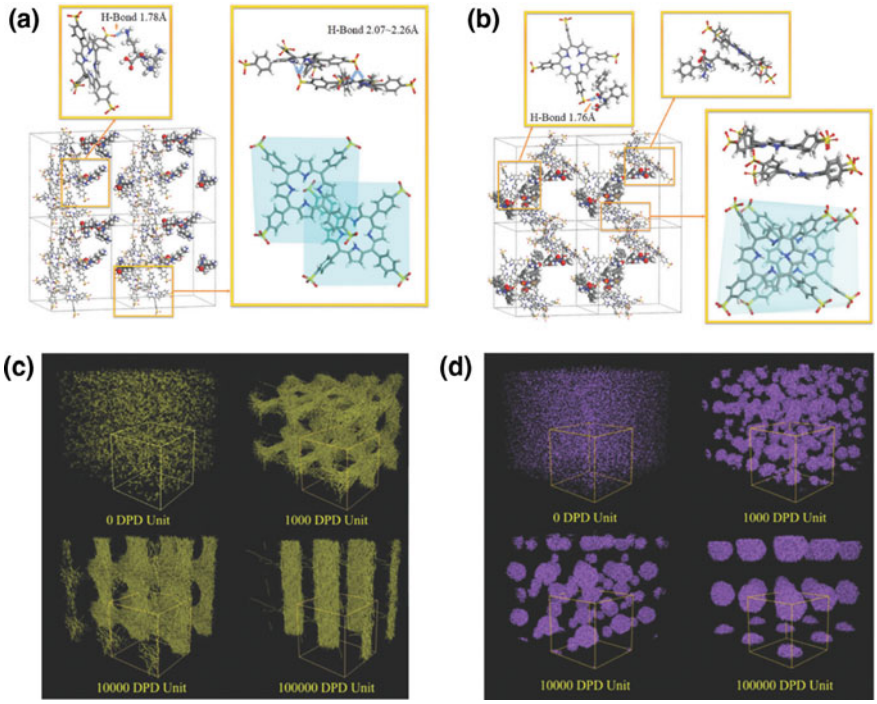

Fig. 7.6 Simulation of peptide-porphyrin hierarchical assembly. Structures of assembled **a** TPPS-KK and **b** TPPS-FF obtained by molecular dynamics simulation. Morphologies of **c** TPPS-KK and **d** TPPS-FF at different simulation times in DPD simulation (Reprinted with permission from Ref. [65]. Copyright 2016, Royal Society of Chemistry)

extinction was observed for two orthogonal fiber bundles at the cross point, suggesting that the nanorods or nanofibers are uniformly distributed on the fiber bundles. Characteristic absorption peak of J-aggregated TPPS was also observed in the fiber bundles, indicating that the TPPS molecules are in J-aggregation. In addition, the chiral signal corresponding to the J-aggregated TPPS increases during the self-assembly process. Similar with FF-promoted self-assembly of TPPS, the KK-promoted self-assembly of TPPS is also a hierarchical organization process. Initially, electrostatic and hydrogen bonding interactions between KK and TPPS promotes the formation of nanorods consisting of J-aggregated porphyrin. Then, the resulting nanorods self-organize at long range to form long fiber bundles.

The self-assembly mechanisms of the dipeptide-porphyrin systems have been further analyzed by multi-scale theoretical study [65]. Molecular dynamics simulation proves that the KK^{3+} molecules are distributed on the surface of H_2TPPS^{2-} nanorods (Fig. 7.6a). The residues of FF^{+} (benzyl groups) are more likely to bind with the J-aggregated H_2TPPS^{2-} nanorods via hydrophobic interaction (Fig. 7.6b). Core–shell structure made of H_2TPPS^{2-} and dipeptides has been constructed by dissipative particle dynamics (DPD) simulation. The KK^{3+} molecules tend to be

released from the interface of the cores, promoting the coalescence of cores, and thus the J-aggregated H_2TPPS^{2-} are better ordered to generate fiber bundles (Fig. 7.6c). When these rods stack together, FF^+ is more likely to create crosslinking, resulting in formation of equilibrium microspheres (Fig. 7.6d).

7.3.2 *Peptide-Modulated Self-assembly of Photosensitizers and Azobenzenes*

Photosensitizers can be excited by light and generate single oxygen to kill tumor cells and tissues in photodynamic therapy (PDT) [66–68]. However, most photosensitizers are poorly soluble in water, which results in low bioavailability [69, 70]. Dispersive nanoparticles of photosensitizers have been constructed by co-assembly of photosensitizers with simple dipeptide or amphiphilic amino acid to as photosensitive drug delivery systems [71]. CDP and 9-Fluorenylmethoxycarbonyl-l-lysine (Fmoc-L-Lys) were used as models of an amphiphilic dipeptide and amino acid, respectively, due to their excellent biocompatibility, nonimmunogenicity, and easy availability. CDP or Fmoc-L-Lys can tune self-assembly of Chlorin e6 (Ce6), a model hydrophobic photosensitive drug, to form uniform nanospheres (Fig. 7.7a, b, c). The Soret band for Ce6 was broadened and red-shifted in the assembled nanodrugs (Fig. 7.7d), indicative of intermolecular hydrophobic and π–π interactions. The nanospheres disassembled at high ionic strength, suggesting the existence of electrostatic forces in the co-assembly process. Therefore, the multiple weak intermolecular interactions, including electrostatic, π–π stacking, and hydrophobic interactions drive the self-assembly.

Tetraphenylethylene (TPE) is a propeller-like molecule with the behavior of aggregation-induced emission (AIE) due to restriction of intramolecular rotations [72]. The emission properties of TPE are usually tailored by using time-consuming organic synthesis. Dynamic regulation of the emission intensity of TPE has been realized by facile peptide-tuned assembly of TPE [73]. After dropping solutions of CDP or Fmoc-L-Lys into TPE-COOH nanoparticle suspensions, the emission of CDP/TPE-COOH nanoparticles has an increase than that of bare TPE-COOH nanoparticles. In contrast, the Fmoc-L-Lys/TPE-COOH nanoparticles show a decreased fluorescence. CDP can enhance the fluorescence presumably due to restriction of intramolecular rotations of TPE molecules via hydrophobic interaction, while Fmoc-L-Lys can weaken the emission of TPE nanoparticles probably due to π–π stack-induced charge transfer.

Photoswitchable sulfonicazobenzene 4-[(4-ethoxy)phenylazo] benzenesulfonic acid (EPABS) was used to manipulate the self-assembly of CDP [74]. The trans-cis conformational change of EPABS induced by light can obviously change the assembled structures of CDP. When EPABS is in the transform, it can co-assemble with CDP into branched structures. After UV irradiation, higher hydrophilic cis-EPABS is formed, leading to disassembly of the structures. The released CDP molecules can form vesicle-like structures via a self-assembly process. Sulfonic

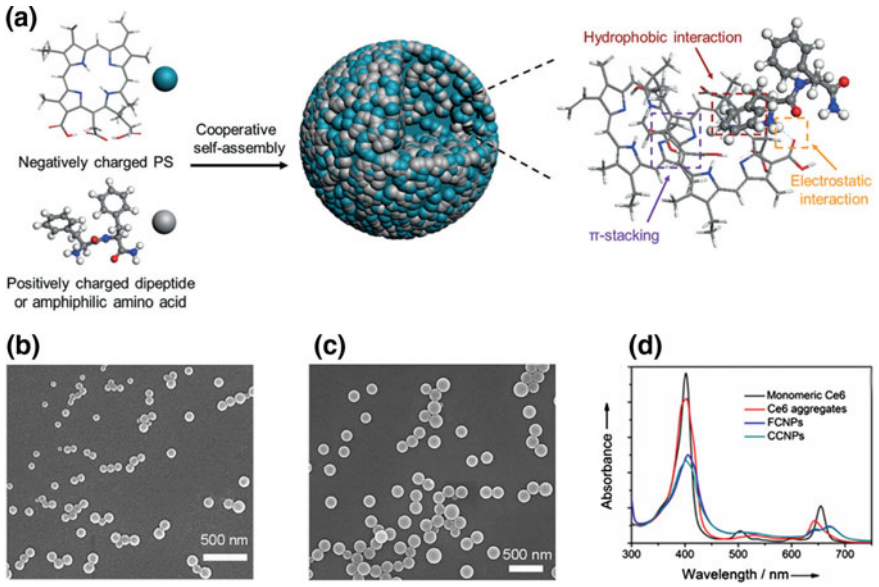

Fig. 7.7 Dipeptide- or amino-acid-tuned self-assembly of photosensitizers (PSs). **a** Schematic illustration. **b** SEM image of assembled nanoparticles using Fmoc-L-Lys and Ce6 as building blocks (FCNPs). **c** SEM image of assembled nanoparticles using CDP and Ce6 as building blocks (CCNPs). **d** Uv–vis absorption spectra of assembled nanoparticles (Reprinted with permission from Ref. [71]. Copyright 2016, Wiley-VCH)

azobenzenes also show a good capability to tune the self-assembly of CDP and diverse assembled structures including urchin-like, flower-like, and plate-like microstructures can be formed [75].

7.4 Self-assembly of Peptide-Inorganic Hybrid Nanomaterials

Self-assembly of peptide-inorganic hybrid nanomaterials is particularly powerful because in such approaches the ease and control offered by the self-assembly of organic components can be combined with the electronic, magnetic or photonic properties of inorganic components.

7.4.1 Peptide-Modulated Self-assembly of Polyoxometalates

POMs are multifunctional nanoclusters of polyatomic ions [76]. Co-assembly of phosphotungstic acid (PTA), a typical POM, with CDP in aqueous solution

generates hybrid spheres with a diameter of about 150 nm (Fig. 7.8a, b) [77]. Energy dispersive X-ray (EDX) spectroscopy on the SEM reveals that the nanospheres are formed by both PTA and CDP. The high-resolution TEM (HR-TEM) imaging shows that the assembled spheres are formed by the organization of peptide-encapsulated clusters (PECs), which consist of single POM clusters and a surrounding peptide shell (Fig. 7.8c). Hence, a hierarchical assembly process is believed responsible for the formation of the nanospheres. FTIR spectra suggest that the initial formation of PECs from PTA and CDP is due to strong electrostatic interactions, while further assembly of PECs is based on multiple non-covalent interactions, including, π–π stacking, hydrophobic effect, and van der Waals forces. It is also found that such nanospheres are able to encapsulate various functional molecules and nanomaterials with distinctive properties, such as positively charged Rhodamine 6G, neutral fluorescein isothiocyanate, negatively charged Congo Red, dextran, hypocrellin B nanoparticles, and hydrophilic gold nanoparticles. The adaptive encapsulation of guest materials is easily realized by adding the guest materials to the solution containing PTA before mixing PTA and CDP. Profoundly, the colloid nanospheres of PTA and CDP are responsive to the stimuli of pH and temperature. Moreover, the transition from nanospheres to surface-supported hybrid films under near-infrared (NIR) irradiation is demonstrated [78]. The versatile encapsulation ability of the nanospheres along with their responsiveness to external stimuli suggests such peptide-inorganic hybrid materials are promising for biomedical applications.

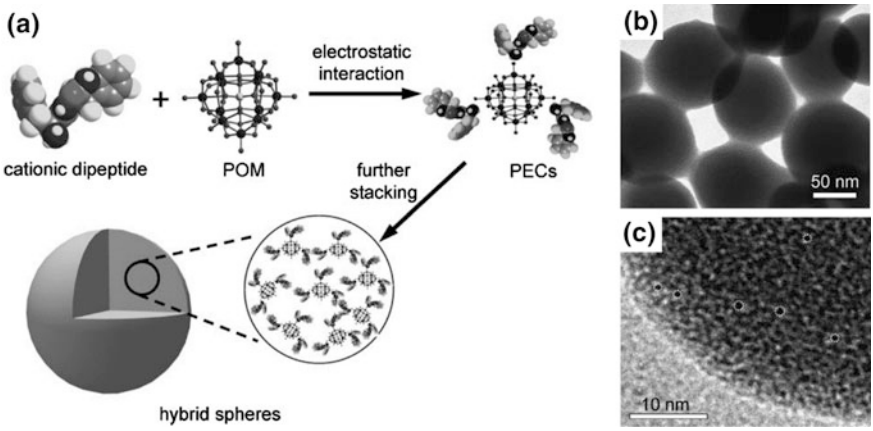

Fig. 7.8 Co-assembly of CDP and POM. **a** Schematic illustration of the formation of the PECs and the hybrid spheres. **b** TEM image of the spheres. **c** HR-TEM image of the spheres showing the PECs (Reprinted with permission from Ref. [77]. Copyright 2010, Wiley-VCH)

7.4.2 Peptide-Modulated Self-assembly of Quantum Dots

Semiconductor QDs are nanoscale particles. Due to their small size, QDs show specific optical and electronic properties [79]. Assembly of such small nanoparticles into higher order architectures while keeping their optical and electronic properties unaffected is of great interest. Supramolecular nanostructures of peptides provide suitable scaffolds to achieve higher order architectures of QDs. The immobilization of QDs by peptides is demonstrated by gelation of a QDs dispersed toluene solution by FF (Fig. 7.9a) [47]. TEM images indicate that most of the QDs are attached to the peptide nanofibers (Fig. 7.9b, c). The gels of the encapsulated QDs show characteristic fluorescence signals of individual QDs though the emission peaks slightly blue-shifted due to the ligand interactions between FF molecules and the QDs (Fig. 7.9c), suggesting that the photophysical properties of the encapsulated QDs remained mainly. Hence, the encapsulation by self-assembled peptide nanostructures provides a suitable method for construction of higher order architectures of QDs.

Since the supramolecular structures of peptides are responsive to external stimuli, the gels of the encapsulated QDs can be manipulated to other architectures [80]. To demonstrate this structural transition for higher order architectures of QDs, gels encapsulated QDs are prepared by gelation of a toluene solution containing QDs by CDP. Then, toluene is removed from the gels by vacuum drying to form the xerogels of encapsulated QDs. By means of adding water to the xerogels and ultrasonic treatment, the xerogels of encapsulated QDs are manipulated to stable nanospheres. In addition, the size of the nanospheres is readily controlled by varying the duration time of ultrasonic treatment and the concentration of CDP. EDX analyses reveal that the colloid nanospheres are composed by both CDP and QDs. The photoluminescence images demonstrate that the assembled QDs in the nanospheres remain their original luminescence properties. Moreover, the colloid nanospheres are stable in a serum-containing cell culture media. When the

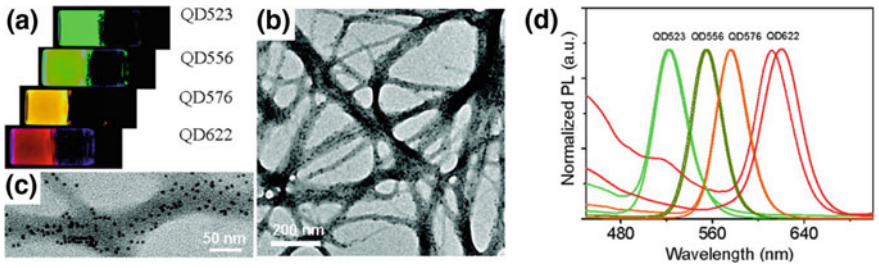

Fig. 7.9 Encapsulation of QDs in FF gel. **a** Photoluminescence photograph of four hybrid gels with different QDs. **b** TEM image of the encapsulated QD523 nanocrystals in the fibril network. **c** Magnified TEM image of the QD523 nanocrystals immobilized to the fibril. **d** Emission spectra of the free QDs in toluene (*solid line*) and the encapsulated QDs in gel (*dash dot*) (Reprinted with permission from Ref. [47]. Copyright 2008, American Chemical Society)

nanopsheres were incubated with HeLa cells, they were successfully internalized by cells and accumulated mainly in the cytoplasm. Cell viability analyses show that the nanospheres are biocompatible at the concentration of 200 μg mL^{-1}. The structural transition of peptide-modulated architectures of QDs along with their high biocompatibility suggest that self-assembling peptides may be widely applicable for construction of biocompatible functional organic–inorganic biomaterials.

7.5 Schiff Base Interaction-Induced Self-assembly of Peptides

In situ generation of peptide-based self-assembling building blocks is realized by Schiff base formation from peptides and GA. It is initially found that CDP and GA assemble into nearly monodisperse nanoparticles with a size of about 450 nm in water gradually when aging the mixture of them at room temperature for about 24 h [81]. The nanoparticles show a positive surface charge, probably due to the presence of positively charged amino groups on their surface. X-ray photoelectron spectroscopy (XPS) spectra reveal that the formed nanoparticles contain carbon–nitrogen double bonds, indicating the formation of Schiff base between the amino group of CDP and the aldehyde group of GA. Spectra of MALDI-TOF mass spectrometry show that the building blocks of the nanoparticles are mainly CDP-2GA-CDP and CDP-3GA-CDP, the products of the reaction of CDP, and oligomeric GA (Fig. 7.10a). Further experiments reveal that the size of the nanoparticles can be controlled by prereaction of CDP and GA in HFIP before the addition of water [82]. When the reaction time for CDP and GA in HFIP is more than 24 h, the size of the obtained nanoparticles drops to 70 nm (Fig. 7.10b, c), suitable for in vivo applications. Mass spectrometry analyses suggest that the variation of building blocks is responsible for the change of the sizes. CDP-2GA-CDP is the main building block for nanoparticles with less prereaction time, while CDP-3GA-CDP is the main building block for nanoparticles with the prereaction of more than 24 h. In addition, the surface change of the nanoparticles can be reversed from positive to negative by surface decorating negatively charged heparin. Such reversion of surface charge by heparin decoration is highly valuable for in vivo applications not only because negatively charged nanoparticles might have a longer circulation time in the bloodstream but also because heparin has been reported as a natural substance that can interfere with tumor metastasis.

GA-induced self-assembly of peptides has also been demonstrated by using FF. Intriguingly, reaction and self-assembly of GA and FF in emulsions of toluene and water follow an interfacially controlled process and are driven by synergistic thermodynamic and kinetic control [83]. At the beginning, the formed nanostructures are crescent-like nanoparticles, which gradually turn into bowl-like nanoparticles along with time and eventually grow into solid interior nanoparticles as the final structures. More sophisticated microstructures can be realized

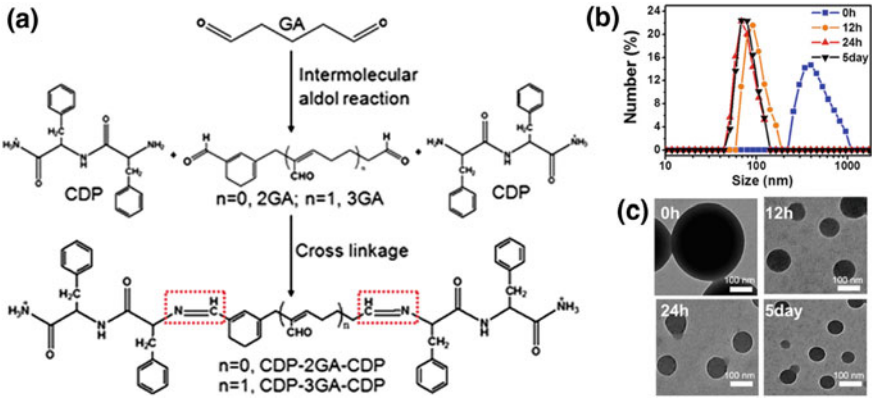

Fig. 7.10 Aldehyde-induced self-assembly of CDP. **a** The formation of CDP-2GA-CDP and CDP-3GA-CDP through reaction between CDP and GA (Reprinted with permission from Ref. [81]. Copyright 2015, Wiley-VCH). **b** Size of the formed nanoparticles under different prereaction times. **c** TEM images of the formed nanoparticles under different prereaction times (Reprinted with permission from Ref. [82]. Copyright 2016, American Chemical Society)

according to the strategy of GA-induced self-assembly of FF by using other emulsions. For instance, multicompartmental hollow spheres have been constructed in emulsions of water/HFIF/hexane [84].

7.6 Applications of Peptide-Based Supramolecular Nanomaterials

Supramolecular peptide nanomaterials have attracted a lot of attentions for biomimetic and biomedical applications due to their advantages of functional diversity and excellent biocompatibility. Nanostructures constructed from peptide-tuned self-assembly of porphyrins have been applied for biomimetic photosystem and photocatalysis. Self-assembled and co-assembled peptide nanoparticles have been evaluated as delivery vehicles for antitumor drugs.

7.6.1 Applications in Biomimetic Photosystem

The FF-TPPS microspheres and KK-TPPS fiber bundles can in situ mineralize Pt nanoparticles via photo-deposition [63, 64]. Porphyrin is excited by light and the resulted anionic porphyrin radical can reduce the K_2PtCl_4 to Pt. After illumination, discrete Pt nanoparticles of 2 nm are formed on the surfaces of the microspheres and Pt nanospheres and Pt nanowires are observed locally on the fiber bundles

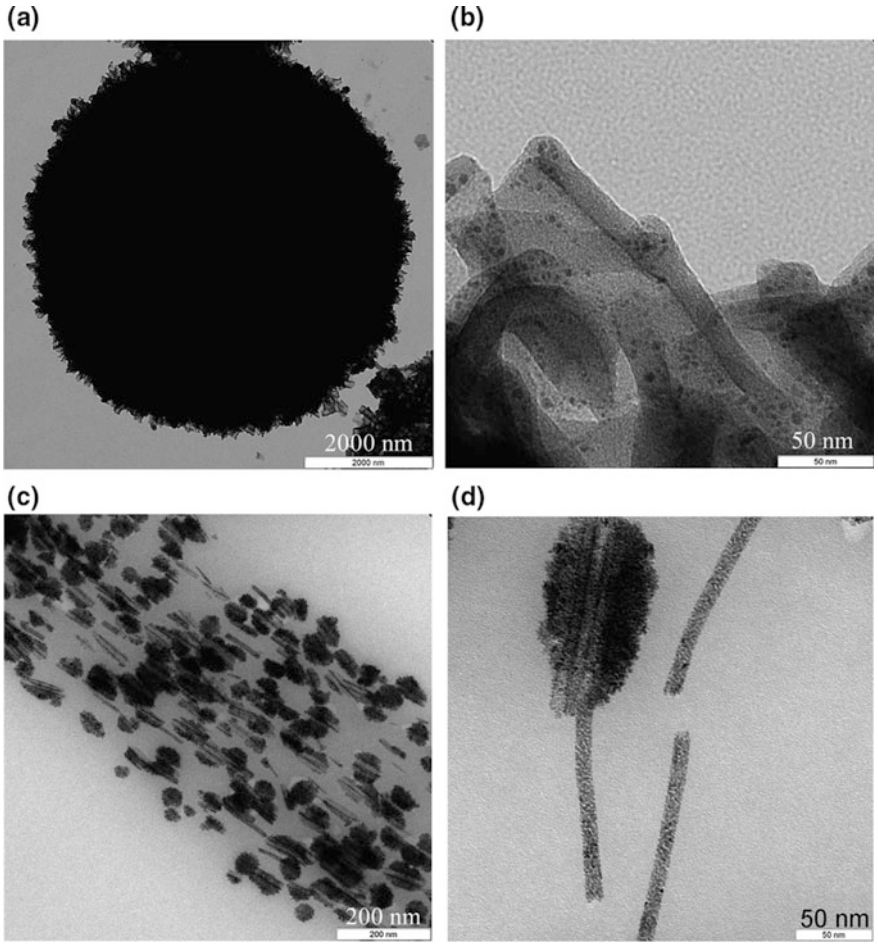

Fig. 7.11 TEM images of the Pt nanomaterials reduced by peptide-porphyrin microspheres or fiber bundles from a photocatalytic pathway. **a** TEM image and **b** higher magnification of Pt incorporated microsphere (Reprinted with permission from Ref. [63]. Copyright 2014, Wiley-VCH). **c** TEM image and **d** higher magnification of Pt nanowires and nanospheres synthesized by fiber bundles (Reprinted with permission from Ref. [64]. Copyright 2015, Wiley-VCH)

(Fig. 7.11). The growth of Pt nanoparticles is oriented along the long axis of the fiber bundles, resulting in the formation of Pt nanowires. In addition, TiO_2 nanoparticles of 5 nm can be mineralized on the surface of the KK-TPPS fibers after incubation with titanium (IV) bis(ammonium lactato)dihydroxide (TiBALDH) in aqueous solution at a high temperature [85]. The HR-TEM analyses show the orientation of the anatase (101) plane. The synthesis of TiO_2 nanoparticles contains several steps. Initially, anionic TiBALDH molecules bind to the amino groups of KK through electrostatic interaction. Subsequently, the mineralization reaction

follows the acid–base catalysis of the peptide molecules, leading to the hydrolysis of the TiBALDH complexes, followed by condensation of trihydroxyl species, and ultimately resulting in the formation of TiO_2.

7.6.2 Applications in Photocatalysis

The FF-TPPS microspheres show photocatalytic capability of oxidation of I^- to I_3^- (Fig. 7.12a) [63]. In addition, the microspheres possess enhanced photostability as compared to the pure J-aggregates under illumination for an extended period of time, as proved by the changes of Soret and Q bands. Thus, the yield of iodide is maintained over longer time in the presence of the microspheres (Fig. 7.12b), suggesting that binding of FF to the $[H_4TPPS]^{2-}$ dianions, or the structural stability of the microstructured matrix, may result in the sustained catalytic performance. The microspheres can also catalyze the conversion of organic matter under illumination, such as photo-reduction of 4-nitrophenol (4-NP) to 4-aminophenol (4-AP) (Fig. 7.12c and d).

The co-assembled KK-TPPS fibers can be flexibly self-functionalized of reaction center (TiO_2/Pt) in a volcanic hydrothermal "prebiotic soup": acidic (pH 2), hot (70 °C), and mineral-containing (Na^+, Ti^{4+}, Pt^{2+}, and so forth) water [85]. The porphyrin in the hierarchical fiber bundles has a similar organization to that of chlorosomes. TiO_2/Pt can be regarded as a primitive reaction center model, which uses the energy from light-harvesting porphyrin assemblies to achieve charge separation and catalyze proton reduction for generation of hydrogen. Thus, such system resembles the architectonics of green sulfur bacteria. After illumination by visible light, H_2-evolution occurs on the hybrid fibers in the prebiotic soup (Fig. 7.13a, b). Integration of TiO_2 and Pt simultaneously into the fibers leads to the biggest hydrogen production rate. Interestingly, the H_2 evolution activity of the hybrid fibers turns out to be dramatically increased by 13 times when increasing the NaCl concentration of the prebiotic soup (Fig. 7.13c), probably due to the enhanced exciton delocalization via NaCl-induced coupling of porphyrin monomers or nanotubular subunits. Additionally, the hybrid fibers show sustainable H_2 production in response to light illumination.

7.6.3 Applications in Biomedicine

The assembled photosensitizer nanodrugs (Fmoc-L-Lys/Ce6) have tunable size, high loading efficiency, and responsiveness to the stimuli of pH, surfactants, and enzymes [71]. Therefore, we evaluate their applications in antitumor PDT. The nanodrugs can be uptaken by tumor cells and disassembled in lysosome to release free drugs (Fig. 7.14a). 3-(4,5-dimethylthiazolyl-2)-2,5-diphenyltetrazolium bromide (MTT) assay shows significantly better anticancer efficacy for the nanodrugs

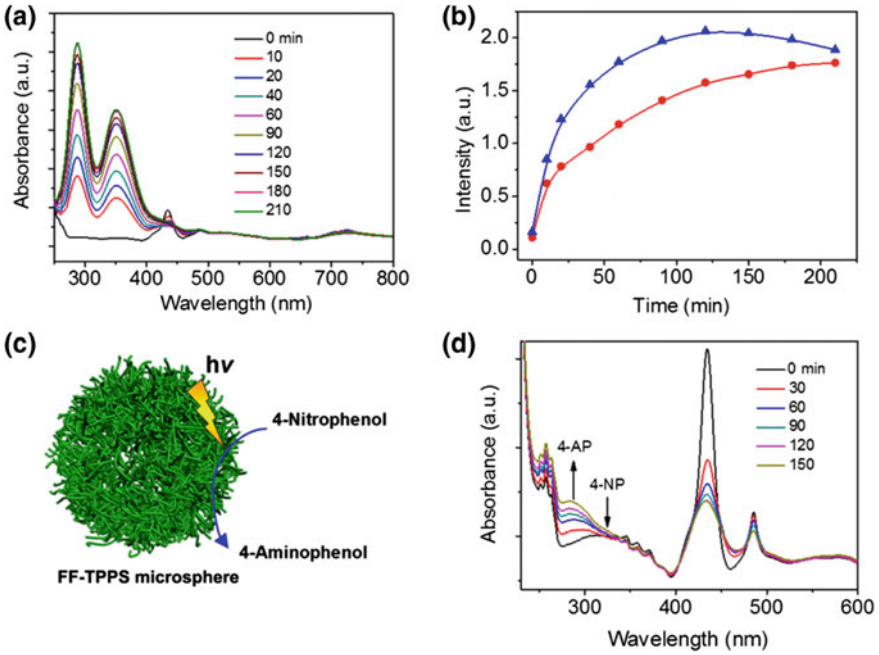

Fig. 7.12 Photocatalysis by FF-TPPS microspheres. **a** UV–vis absorption spectra showing time-dependent changes corresponding to product formation under irradiation of sodium iodide. **b** Plots of intensity at 353 nm versus irradiation time for tri-iodide formation in the presence of a dispersion of the microspheres (*red*) or TPPS J-aggregates (*blue*). **c** Illustration of photocatalytic reduction of 4-nitrophenol (4-NP) into 4-aminophenol (4-AP) in the presence of a dispersion of the microspheres. **d** Time-dependent UV–vis absorption spectra showing the production of 4-AP from 4-NP in the presence of the microspheres (Reprinted with permission from Ref. [63]. Copyright 2014, Wiley-VCH)

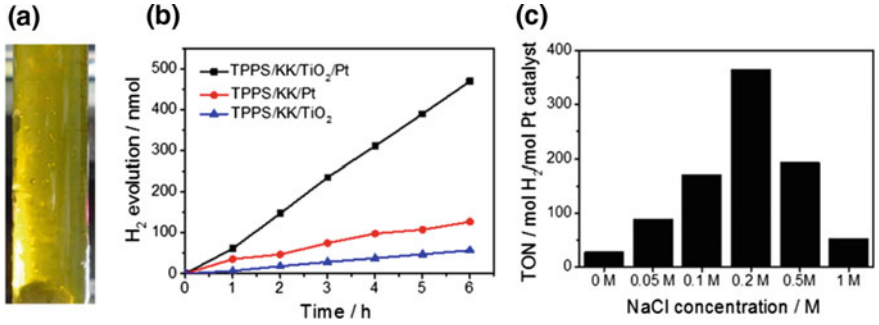

Fig. 7.13 Photocatalytic hydrogen evaluation by TPPS/KK/TiO_2/Pt fibers. **a** Photograph of H_2 bubbles produced from the hybrid fibers in the test tube during illumination. **b** Time dependence of the H_2 production of TPPS/KK/Pt, TPPS/KK/TiO_2 and TPPS/KK/TiO_2/Pt fibers. **c** Effect of NaCl on the hydrogen production of the hybrid fibers (Reprinted with permission from Ref. [85]. Copyright 2016, Wiley-VCH)

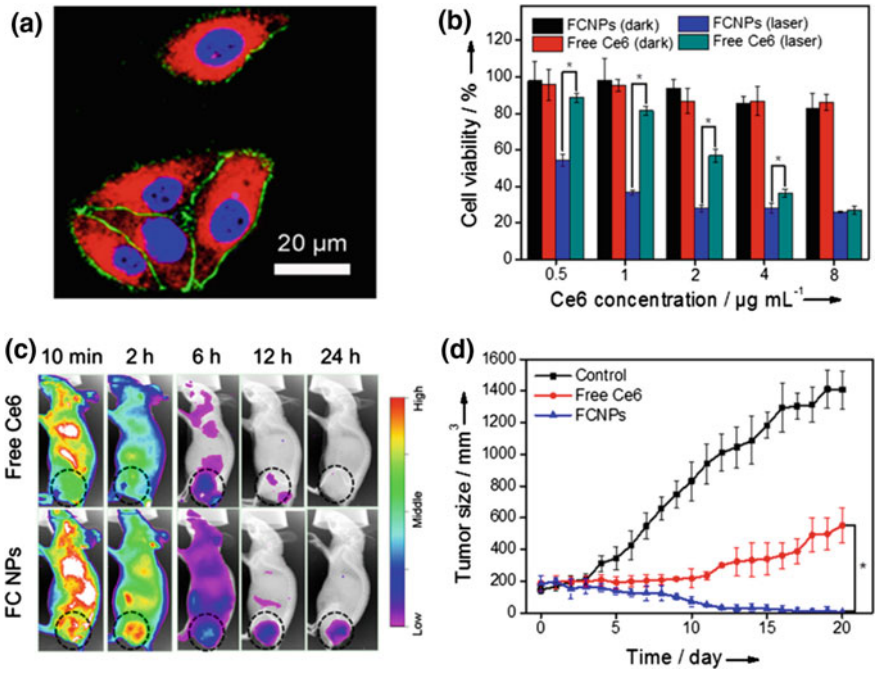

Fig. 7.14 Amphiphilic dipeptide- or amino-acid-tuned self-assembly of photosensitizers for in vitro and in vivo PDT. **a** Internalization of the assembled FCNPs by MCF7 cells. The *red* staining is from the photosensitizer while nuclei are stained by *blue* and cell membrane is stained by *green*. **b** In vitro cytotoxicity and photocytotoxicity of FCNPs. **c** Fluorescence images of tumor-bearing mice showing in vivo distribution of FCNPs and free Ce6. **d** Tumor growth curves of the mice in different groups (Reprinted with permission from Ref. [71]. Copyright 2016, Wiley-VCH)

than free drug (Fig. 7.14b). No cytotoxicity was observed in the dark, confirming the good biocompatibility of the nanodrugs. The nanodrugs also show preferable biodistribution. After intravenous injection, the nanodrugs exhibited sustained and stronger Ce6 fluorescence at the tumor site than free drugs (Fig. 7.14c), mainly due to the enhanced permeability and retention (EPR) effect [86]. These therapeutic features result in good PDT efficacy in vivo, leading to almost complete tumor inhibition after receiving only a single treatment (Fig. 7.14d).

Nanoparticles constructed from GA-induced self-assembly of CDP are versatile drug delivery vehicles for both chemotherapy and PDT. GA/CDP nanoparticles show a loading efficiency of more than 50% in encapsulation of doxorubicin (DOX), a chemotherapy drug [81]. The release rate of DOX from the GA/CDP-DOX nanoparticles is responsive to enzymes. In phosphate-buffered saline solution, only about $12.7 \pm 0.3\%$ of the loaded DOX is released within 10 days. In contrast, $75.3 \pm 1.4\%$ of the loaded DOX is released in the presence of tyrisin, due to enzyme-induced degradation of GA/CDP nanoparticles.

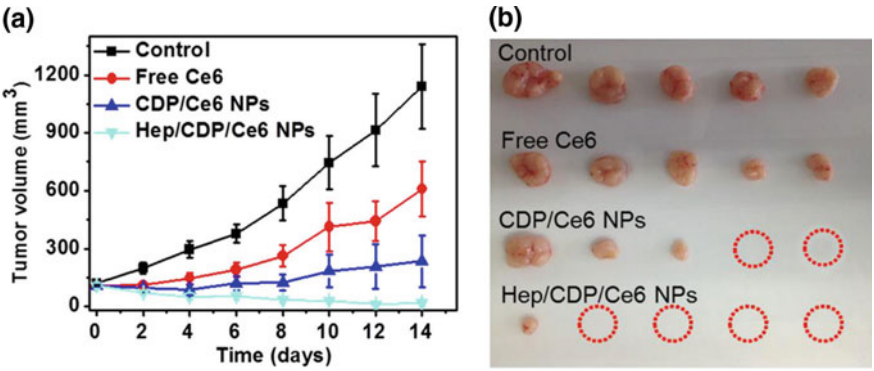

Fig. 7.15 Nanoparticles self-assembled from GA and CDP as drug delivery vehicles of Ce6 toward antitumor PDT. **a** Tumor growth profiles in MCF-7 tumor-bearing mice during PDT. **b** Photographs of the isolated tumors at the end of experiment. The eliminated tumors were expressed in *red circles* (Reprinted with permission from Ref. [82]. Copyright 2016, American Chemical Society)

Significantly, GA/CDP-DOX nanoparticles exhibit a better inhibition capacity toward HeLa cells than the equivalent dose of free DOX, especially at the low concentration of DOX. Also, GA/CDP nanoparticles with a smaller size and surface heparin decoration are demonstrated as efficient drug delivery vehicles for Ce6 [82]. In vivo PDT results show that the drug-loaded nanoparticles (Hep/CDP/Ce6 NPs) are efficient in inhibition of MCF-7 tumors (Fig. 7.15).

7.7 Summary

In summary, peptide-based supramolecular chemistry, including self-assembly of peptides and peptide-modulated self-assembly of functional components have been widely investigated for controllable fabrication of advanced micro- and nanomaterials. Peptide-based materials show tremendous potential for biomimetic and biomedical applications with advantages of tunable micro- and nanostructures and corresponding functions, ease of incorporating organic and inorganic materials, and customized responsiveness to external stimuli. Particularly, hierarchical assembly and structural transition of peptide-based micro- and nanomaterials can be readily realized by manipulation of the non-covalent interactions at different organization levels, providing the formed materials with increasing higher ordered architectures and corresponding functions. As a special kind of peptide-based materials, peptide crystals have shown intriguing optical waveguiding capability promising for optical bio-applications.

Although peptide-based supramolecular chemistry and materials have been significantly promoted by successful examples of both experimental and theoretical

studies, there are still formidable challenges in tailored fabrication of peptide-based functional materials for biomimetic and biomedical applications. Even for short peptides, such as dipeptides, the prediction of their self-assembly behavior at various conditions has not been fully realized. Hence, more experiment-based simulations are needed to reveal relationships among environmental parameters, non-covalent interactions, nano- and microstructures, and morphology from the molecular level to material level. With respect to applications in biomimetic energy, integration of more functional units, such as various pigments, charge separators, and reaction centers in the process of peptide-modulated assembly is highly desired in order to mimic the complexity and functions of natural photosystems. For biomedical applications, future clinical translation of peptide-based nanomaterials relies on comprehensive evaluation of their biocompatibility and efficiency in vivo, for example, through the pharmacokinetic and pharmacodynamic analysis. Also, introducing antimicrobial, anticancer, and immunomodulatory sequences into the peptide building blocks is expected to be an efficient method to construct peptide-based functional biomaterials.

Acknowledgements The authors acknowledge financial support from the National Natural Science Foundation of China (Project Nos. 21522307, 21473208, 91434103, and 51403214), the Chinese Academy of Sciences (CAS, Project No. QYZDB-SSW-JSC034), and the Talent Fund of the Recruitment Program of Global Youth Experts.

References

1. Askarieh G, Hedhammar M, Nordling K et al (2010) Self-assembly of spider silk proteins is controlled by a pH-sensitive relay. Nature 465:236–238
2. Ybe JA, Brodsky FM, Hofmann K et al (1999) Clathrin self-assembly is mediated by a tandemly repeated superhelix. Nature 399:371–375
3. Yonekura K, Maki S, Morgan DG et al (2000) The bacterial flagellar cap as the rotary promoter of flagellin self-assembly. Science 290:2148–2152
4. Tanaka S, Kerfeld CA, Sawaya MR et al (2008) Atomic-level models of the bacterial carboxysome shell. Science 319:1083–1086
5. van den Ent F, Amos LA, Lowe J (2001) Prokaryotic origin of the actin cytoskeleton. Nature 413:39–44
6. Luger K, Mader AW, Richmond RK et al (1997) Crystal structure of the nucleosome core particle at 2.8 angstrom resolution. Nature 389:251–260
7. Shih WM (2015) Exploiting weak interactions in DNA self-assembly. Science 347:1417–1418
8. Cerny J, Hobza P (2007) Non-covalent interactions in biomacromolecules. Phys Chem Chem Phys 9:5291–5303
9. Zhang SG (2003) Fabrication of novel biomaterials through molecular self-assembly. Nat Biotechnol 21:1171–1178
10. Hartgerink JD, Beniash E, Stupp SI (2001) Self-assembly and mineralization of peptide-amphiphile nanofibers. Science 294:1684–1688
11. Habibi Y, Lucia LA, Rojas OJ (2010) Cellulose nanocrystals: chemistry, self-assembly, and applications. Chem Rev 110:3479–3500

12. Kuzyk A, Schreiber R, Fan ZY et al (2012) DNA-based self-assembly of chiral plasmonic nanostructures with tailored optical response. Nature 483:311–314
13. Zou QL, Liu K, Abbas M et al (2016) Peptide-modulated self-assembly of chromophores toward biomimetic light-harvesting nanoarchitectonics. Adv Mater 28:1031–1043
14. Stupp SI (2010) Self-Assembly and biomaterials. Nano Lett 10:4783–4786
15. Chen CJ, Liu K, Li JB et al (2015) Functional architectures based on self-assembly of bio-inspired dipeptides: structure modulation and its photoelectronic applications. Adv Colloid Interface Sci 225:177–193
16. Percec V, Dulcey AE, Balagurusamy VSK et al (2004) Self-assembly of amphiphilic dendritic dipeptides into helical pores. Nature 430:764–768
17. Shu SJ, Sun L, Zhang XG et al (2011) Polysaccharides-based polyelectrolyte nanoparticles as protein drugs delivery system. J Nanopart Res 13:3657–3670
18. Rest C, Kandanelli R, Fernandez G (2015) Strategies to create hierarchical self-assembled structures via cooperative non-covalent interactions. Chem Soc Rev 44:2543–2572
19. Mann S (2009) Self-assembly and transformation of hybrid nano-objects and nanostructures under equilibrium and non-equilibrium conditions. Nat Mater 8:781–792
20. Groschel AH, Walther A, Lobling TI et al (2013) Guided hierarchical co-assembly of soft patchy nanoparticles. Nature 503:247–251
21. Xing RR, Jiao TF, Liu YM et al (2016) Co-assembly of graphene oxide and albumin/photosensitizer nanohybrids towards enhanced photodynamic therapy. Polymers 8:181
22. Sharma J, Chhabra R, Cheng A et al (2009) Control of self-assembly of DNA tubules through integration of gold nanoparticles. Science 323:112–116
23. Yan H, Park SH, Finkelstein G et al (2003) DNA-templated self-assembly of protein arrays and highly conductive nanowires. Science 301:1882–1884
24. Ercole F, Davis TP, Evans RA (2010) Photo-responsive systems and biomaterials: photochromic polymers, light-triggered self-assembly, surface modification, fluorescence modulation and beyond. Polym Chem 1:37–54
25. Zimenkov Y, Dublin SN, Ni R et al (2006) Rational design of a reversible pH-responsive switch for peptide self-assembly. J Am Chem Soc 128:6770–6771
26. Zhang SG (2012) Lipid-like self-assembling peptides. Acc Chem Res 45:2142–2150
27. Adler-Abramovich L, Gazit E (2014) The physical properties of supramolecular peptide assemblies: from building block association to technological applications. Chem Soc Rev 43:6881–6893
28. Frederix PWJM, Scott GG, Abul-Haija YM et al (2015) Exploring the sequence space for (tri-)peptide self-assembly to design and discover new hydrogels. Nat Chem 7:30–37
29. Zhou J, Du XW, Yamagata N et al (2016) Enzyme-instructed self-assembly of small D-peptides as a multiple-step process for selectively killing cancer cells. J Am Chem Soc 138:3813–3823
30. Martinek TA, Hetenyi A, Fulop L et al (2006) Secondary structure dependent self-assembly of beta-peptides into nanosized fibrils and membranes. Angew Chem Int Edit 45:2396–2400
31. Aggeli A, Bell M, Boden N et al (1997) Responsive gels formed by the spontaneous self-assembly of peptides into polymeric beta-sheet tapes. Nature 386:259–262
32. Smith KH, Tejeda-Montes E, Poch M et al (2011) Integrating top-down and self-assembly in the fabrication of peptide and protein-based biomedical materials. Chem Soc Rev 40:4563–4577
33. De Santis E, Ryadnov MG (2015) Peptide self-assembly for nanomaterials: the old new kid on the block. Chem Soc Rev 44:8288–8300
34. Cui HG, Webber MJ, Stupp SI (2010) Self-assembly of peptide amphiphiles: from molecules to nanostructures to biomaterials. Biopolymers 94:1–18
35. Gazit E (2007) Self-assembled peptide nanostructures: the design of molecular building blocks and their technological utilization. Chem Soc Rev 36:1263–1269

36. Matson JB, Stupp SI (2012) Self-assembling peptide scaffolds for regenerative medicine. Chem Commun 48:26–33
37. Fernandez-Lopez S, Kim HS, Choi EC et al (2001) Antibacterial agents based on the cyclic D, L-alpha-peptide architecture. Nature 412:452–455
38. Kim S, Kim JH, Lee JS et al (2015) Beta-sheet-forming, self-assembled peptide nanomaterials towards optical, energy, and healthcare applications. Small 11:3623–3640
39. Mandal D, Shirazi AN, Parang K (2014) Self-assembly of peptides to nanostructures. Org Biomol Chem 12:3544–3561
40. Wang J, Liu K, Xing RR et al (2016) Peptide self-assembly: thermodynamics and kinetics. Chem Soc Rev 45:5589–5604
41. Zhang SG, Marini DM, Hwang W et al (2002) Design of nanostructured biological materials through self-assembly of peptides and proteins. Curr Opin Chem Biol 6:865–871
42. Stendahl JC, Rao MS, Guler MO et al (2006) Intermolecular forces in the self-assembly of peptide amphiphile nanofibers. Adv Funct Mater 16:499–508
43. Reches M, Gazit E (2003) Casting metal nanowires within discrete self-assembled peptide nanotubes. Science 300:625–627
44. Yan XH, Zhu PL, Li JB (2010) Self-assembly and application of diphenylalanine-based nanostructures. Chem Soc Rev 39:1877–1890
45. Tao K, Levin A, Adler-Abramovich L et al (2016) Fmoc-modified amino acids and short peptides: simple bio-inspired building blocks for the fabrication of functional materials. Chem Soc Rev 45:3935–3953
46. Amdursky N, Molotskii M, Gazit E et al (2010) Elementary building blocks of self-assembled peptide nanotubes. J Am Chem Soc 132:15632–15636
47. Yan XH, Cui Y, He Q et al (2008) Organogels based on self-assembly of diphenylalanine peptide and their application to immobilize quantum dots. Chem Mater 20:1522–1526
48. Su Y, Yan XH, Wang AH et al (2010) A peony-flower-like hierarchical mesocrystal formed by diphenylalanine. J Mater Chem 20:6734–6740
49. Su Y, He Q, Yan XH et al (2011) Peptide mesocrystals as templates to create an Au surface with stronger surface-enhanced Raman spectroscopic properties. Chem Eur J 17:3370–3375
50. Du MC, Zhu PL, Yan XH et al (2011) Honeycomb self-assembled peptide scaffolds by the breath figure method. Chem Eur J 17:4238–4245
51. Yan XH, He Q, Wang KW et al (2007) Transition of cationic dipeptide nanotubes into vesicles and oligonucleotide delivery. Angew Chem Int Edit 46:2431–2434
52. Yan XH, Cui Y, He Q et al (2008) Reversible transitions between peptide nanotubes and vesicle-like structures including theoretical modeling studies. Chem Eur J 14:5974–5980
53. Liu XC, Zhu PL, Fei JB et al (2015) Synthesis of peptide-based hybrid nanobelts with enhanced color emission by heat treatment or water induction. Chem Eur J 21:9461–9467
54. Zhu PL, Yan XH, Su Y et al (2010) Solvent-induced structural transition of self-assembled dipeptide: from organogels to microcrystals. Chem Eur J 16:3176–3183
55. Knowles TP, Fitzpatrick AW, Meehan S et al (2007) Role of intermolecular forces in defining material properties of protein nanofibrils. Science 318:1900–1903
56. Krone MG, Hua L, Soto P et al (2008) Role of water in mediating the assembly of Alzheimer amyloid-beta a beta 16-22 protofilaments. J Am Chem Soc 130:11066–11072
57. Wang J, Liu K, Yan LY et al (2016) Trace solvent as a predominant factor to tune dipeptide self-assembly. ACS Nano 10:2138–2143
58. Yan XH, Su Y, Li JB et al (2011) Uniaxially oriented peptide crystals for active optical waveguiding. Angew Chem Int Edit 50:11186–11191
59. Li YX, Yan LY, Liu K et al (2016) Solvothermally mediated self-assembly of ultralong peptide nanobelts capable of optical waveguiding. Small 12:2575–2579
60. Yan XH, Li JB, Mowald H (2011) Self-assembly of hexagonal peptide microtubes and their optical waveguiding. Adv Mater 23:2796–2801
61. Li Q, Jia Y, Dai LR et al (2015) Controlled rod nanostructured assembly of diphenylalanine and their optical waveguide properties. ACS Nano 9:2689–2695

62. Li Q, Ma HC, Wang AH et al (2015) Self-assembly of cationic dipeptides forming rectangular microtubes and microrods with optical waveguiding properties. Adv Opt Mater 3:194–198
63. Zou QL, Zhang L, Yan XH et al (2014) Multifunctional porous microspheres based on peptide-porphyrin hierarchical co-assembly. Angew Chem Int Ed 53:2366–2370
64. Liu K, Xing RR, Chen CJ et al (2015) Peptide-induced hierarchical long-range order and photocatalytic activity of porphyrin assemblies. Angew Chem Int Ed 54:500–505
65. Liu K, Kang Y, Ma G et al (2016) Molecular and mesoscale mechanism for hierarchical self-assembly of dipeptide and porphyrin light-harvesting system. Phys Chem Chem Phys 18:16738–16747
66. Yano S, Hirohara S, Obata M et al (2011) Current states and future views in photodynamic therapy. J Photochem Photobiol C 12:46–67
67. Xing RR, Liu K, Jiao TF et al (2016) An injectable self-assembling collagen-gold hybrid hydrogel for combinatorial antitumor photothermal/photodynamic therapy. Adv Mater 28:3669–3676
68. Zhang N, Zhao FF, Zou QL et al (2016) Multitriggered tumor-responsive drug delivery vehicles based on protein and polypeptide coassembly for enhanced photodynamic tumor ablation. Small 12:5936–5943
69. Lucky SS, Soo KC, Zhang Y (2015) Nanoparticles in photodynamic therapy. Chem Rev 115:1990–2042
70. Zhang RY, Xing RR, Jiao TF et al (2016) Carrier-free, chemophotodynamic dual nanodrugs via self-assembly for synergistic antitumor therapy. ACS Appl Mater Interfaces 8:13262–13269
71. Liu K, Xing RR, Zou QL et al (2016) Simple peptide-tuned self-assembly of photosensitizers towards anticancer photodynamic therapy. Angew Chem Int Ed 55:3036–3039
72. Wang J, Mei J, Hu RR et al (2012) Click synthesis, aggregation-induced emission, E/Z isomerization, self-organization, and multiple chromisms of pure stereoisomers of a tetraphenylethene-cored luminogen. J Am Chem Soc 134:9956–9966
73. Liu K, Zhang RR, Li YX et al (2016) Tunable aggregation-induced emission of tetraphenylethylene via short peptide-directed self-assembly. Adv Mater Interfaces 4:1600183
74. Ma HC, Fei JB, Li Q et al (2015) Photo-induced reversible structural transition of cationic diphenylalanine peptide self-assembly. Small 11:1787–1791
75. Ma HC, Fei JB, Cui Y et al (2013) Manipulating assembly of cationic dipeptides using sulfonic azobenzenes. Chem Commun 49:9956–9958
76. Cronin L, Muller A (2012) From serendipity to design of polyoxometalates at the nanoscale, aesthetic beauty and applications. Chem Soc Rev 41:7333–7334
77. Yan XH, Zhu PL, Fei JB et al (2010) Self-assembly of peptide-inorganic hybrid spheres for adaptive encapsulation of guests. Adv Mater 22:1283–1287
78. Xing RR, Jiao TF, Feng L et al (2015) Photothermally-induced molecular self-assembly of macroscopic peptide-inorganic hybrid films. Sci Adv Mater 7:1701–1707
79. Alivisatos AP (1996) Semiconductor clusters, nanocrystals, and quantum dots. Science 271:933–937
80. Yan XH, Cui Y, Qi W et al (2008) Self-assembly of peptide-based colloids containing lipophilic nanocrystals. Small 4:1687–1693
81. Zhang H, Fei JB, Yan XH et al (2015) Enzyme-responsive release of doxorubicin from monodisperse dipeptide-based nanocarriers for highly efficient cancer treatment in vitro. Adv Funct Mater 25:1193–1204
82. Ma K, Xing RR, Jiao TF et al (2016) Injectable self-assembled dipeptide-based nanocarriers for tumor delivery and effective in vivo photodynamic therapy. ACS Appl Mater Interfaces 8:30759–30767
83. Wang J, Shen GZ, Ma K et al (2016) Dipeptide concave nanospheres based on interfacially controlled self-assembly: from crescent to solid. Phys Chem Chem Phys 18:30926–30930
84. Li Q, Ma HC, Jia Y et al (2015) Facile fabrication of diphenylalanine peptide hollow spheres using ultrasound-assisted emulsion templates. Chem Commun 51:7219–7221

85. Liu K, Xing RR, Li YX et al (2016) Mimicking primitive photobacteria: sustainable hydrogen evolution based on peptide–porphyrin co-assemblies with a self-mineralized reaction center. Angew Chem Int Ed 55:12503–12507
86. Petros RA, DeSimone JM (2010) Strategies in the design of nanoparticles for therapeutic applications. Nat Rev Drug Discovery 9:615–627